ORNL/SPR-2019/1335

Impact of Control Blade Insertion on the Deformation Behavior of SiC-SiC Channel Boxes in Boiling Water Reactors

Nuclear Technology Research and Development

Prepared for
US Department of Energy
Advanced Fuels Campaign
G. Singh[1], J. P. Gorton[1,2], D. Schappel[1,2],
B. S. Collins[2], N. R. Brown[1], and B. D. Wirth[1,2]
[1]University of Tennessee Knoxville
[2]Oak Ridge National Laboratory
September 27, 2019
M3FT-19OR020201065

SUMMARY

This report describes the analysis of distortion of a Silicon carbide fiber-reinforced silicon carbide matrix (SiC-SiC) composite channel box under in-reactor conditions of a boiling water reactor (BWR). The BWR core has significant gradients in the fast neutron flux across the channel box due to the presence of water rods within the fuel assemblies, and these gradients increase further with the insertion of control blades. As a result of temperature and neutron flux dependent irradiation induced swelling of SiC, the SiC-SiC composite channel box can undergo significant distortion. In this work, we evaluate the SiC-SiC channel box distortion for three different control blade positions. This analysis is based on the neutron flux and temperature distributions in the BWR core calculated using the neutronics code MPACT and thermal-hydraulics code CTF. This calculation is coupled through temperature feedback. Subsequently, we have performed structural analysis based on the calculated neutron flux and temperature distributions, to determine the deformation and stress development in the channel box. The structural analysis was performed using the fuel performance modeling code BISON and the commercial finite element analysis software Abaqus.

The results indicate that the channel box will undergo time dependent lateral bowing for all the control blade positions in the assembly. The bowing behavior is dominated by the swelling of SiC-SiC material under non-uniform neutron flux, and changes with variation in the control blade position. The lateral bending will cause a temporary interference between the channel box and the control blade. The developed stresses exceed the proportional limit stress of the material, which may cause matrix microcracking in the channel box. However, the stresses remain below the ultimate tensile strength of the material, and therefore, development of a full, through thickness crack in the channel box is not expected.

This page is intentionally left blank.

CONTENTS

This page is intentionally left blank.

FIGURES

Tables

ACRONYMS

ATF	Accident Tolerant Fuel
BWR	Boiling Water Reactor
CASL	Consortium for Advanced Simulation of Light Water Reactors
SiC	Silicon Carbide

Impact of Control Blade Insertion on the Deformation Behavior of SiC-SiC Channel Boxes in Boiling Water Reactors

1. INTRODUCTION

In the series of events that led to the 2011 Fukushima Daiichi nuclear power plant accident, the highly exothermic reaction between the steam and Zirconium alloy cladding and core structures was a significant contributor to the accident. This reaction led to release of a massive amount of heat and generation of hydrogen gas. The hydrogen gas explosion broke the containment structure and released the radionuclides into the open environment. Since that accident there have been concerted efforts throughout the world to develop so-called 'accident tolerant fuel' systems (ATF) which provide greater resistance to beyond design basis accidents and enhanced coping time. In pursuit of new materials for these ATF systems, silicon carbide (SiC) reinforced silicon carbide matrix composite material (SiC-SiC) has been identified as a promising material for fuel cladding and core structures.

The attractive materials properties of SiC-SiC for reactor core applications include 1) radiation stability, 2) lack of progressive irradiation growth [1, 2], 3) general chemical inertness and 4) ability to maintain structural strength at elevated temperatures [3]. Additionally, SiC exhibits 5) low decay heat and 6) a lower neutron absorption cross-section than Zirconium. A comprehensive discussion on the properties of nuclear grade SiC-SiC is provided in Ref. by Katoh et al. [4]. There has been considerable research and development work towards the application of SiC-SiC as fuel cladding or core structure material. Probably the earliest study showing the advantage of SiC cladding over traditional Zirconium alloy cladding was conducted by Johnson et al. [5], which modeled the performance of SiC cladding in Three Mile Island reactor 2 severe accident and station blackout accident (SBO) of a four-loop Westinghouse PWR. The results showed that significantly lower peak fuel temperature, less hydrogen production and less generation of molten metal would occur if SiC cladding replaced the traditional Zirconium alloy cladding. Sebe et al. [6], Heerden et al. [7] and Ikegawa et al. [8] have shown similar advantages of SiC over Zirconium alloy for cladding applications.

It should be noted that channel boxes surrounding the fuel assemblies constitute about 40% of Zirconium alloy used in a typical BWR core [9]. Hence replacing the traditional Zircaloy channel boxes with either SiC-SiC composite channel boxes or other alternative would provide a significant benefit in the development of accident tolerant reactors. Compared to cladding application, there have been limited studies on SiC-SiC material for channel box application in boiling water reactors (BWR). Horie et al. performed severe accident analysis of SiC channel box and compared its performance with Zirconium alloy (Zry) channel box for the conditions of Advanced Boiling Water Reactor (ABWR) [10]. The analysis was performed using the Modular Accident Analysis Program (MAAP) code for chemical reaction characteristics and the Toshiba version Transient Reactor Analysis Code (TRAC) for thermal hydraulics analysis. The authors considered four cases of channel box/cladding material: 1) SiC/SiC 2) Zry/Zry 3) SiC/Zry and 4) Zry/SiC. The analysis showed that the amount of hydrogen generated for the SiC/SiC case was about 7-8 times less than Zry/Zry. Several relevant experimental studies and the current status of SiC channel box technology have been documented in Refs. [9, 11-13].

An earlier study on SiC-SiC channel box deformation for BWR applications has shown that the channel box will undergo significant lateral bending, although most of the lateral bending is transient and can recover with straightening of the channel box at later times [14]. The lateral bending is caused by differential swelling across the width of the channel box. The non-uniform fast neutron flux contributes most towards generating these swelling gradients, with small effects from non-uniform temperature distributions.

However, this study considered a situation where the cruciform control blade was fully withdrawn. For other control blade positions, there can be sharp neutron flux gradients and the bowing behavior of the channel box may be substantially different.

The study presented here extends this previous study [14] and is aimed at understanding the effect of different control blade positions on the channel box bowing behavior and evaluating the severity of any interference between the control blade and channel box. The previous study used uncoupled computer codes to calculate the temperature and neutron flux distributions, which cause deformation of SiC-SiC from non-uniform thermal expansion and swelling. The current study employs an improved neutronic-to-thermal-hydraulic code coupling methodology to calculate the temperature and neutron flux distributions in SiC-SiC channel box. A special coupled version of neutronics code MPACT (from the Consortium for Advanced Simulation of Light Water Reactors (CASL)) [15] and the sub-channel thermal hydraulic code CTF [16] were used for this analysis. Because a coupled methodology was used, the fast flux and temperature distributions predicted by MPACT/CTF are expected to be more accurate than the distributions predicted in the previous study [14], which used Serpent [17] and CTF in a decoupled fashion.

A representative GE14 10x10 fuel assembly channel box operating under normal reactor conditions [18] is considered in this work. Three control blade positions – withdrawn, half-inserted and fully inserted into the assembly, are considered. The boundary conditions modeled are that of a fuel assembly located near the core center. The structural analysis is performed using the fuel performance code BISON [19] (commit number: bison-devel-1ed01aecee5052e43f323bd176e85b10aa43d9e1) and the commercial finite element code Abaqus [20] (version 2018).

2. METHOD

Three cases based on the position of control blade in the channel box assembly were analyzed in this work: 1) control blade fully withdrawn (case W), 2) control blade inserted halfway into the assembly (case H) and 3) control blade fully inserted into the assembly (case F). The fast neutron flux is calculated from the total neutron flux based on the chosen energy cutoff values. Two different values of the fast neutron energy cutoff (0.067 MeV and 0.183 MeV) were considered in the analysis to understand the sensitivity of results to the energy cutoff values.

2.1 CONSTITUTIVE MODEL

The channel box material SiC-SiC can undergo deformation in several ways when subjected to the in-reactor environment of a BWR. The primary deformation of SiC-SiC under the influence of neutron irradiation occurs through irradiation induced swelling. The magnitude of the swelling strain has an inverse temperature dependence, with a larger swelling magnitude observed at lower irradiation temperatures [4, 21]. This swelling strain ($\boldsymbol{\varepsilon}^{s}$) saturates at ~1 displacement per atom (dpa) for irradiation temperatures below about 1000°C. Further details about the mechanism of swelling in SiC can be found elsewhere [2]. The secondary modes of deformation are thermal expansion and creep. Of thermal expansion ($\boldsymbol{\varepsilon}^{th}$) and creep deformation ($\boldsymbol{\varepsilon}^{c}$), thermal expansion dominates. The material undergoes creep deformation under the influence of stress and irradiation. Note that the thermal creep, which is induced by the stress and elevated temperatures, is not activated in SiC-SiC until temperatures of ~1500°C [22], and is not considered in the current analysis. Under the influence of mechanical loads, the material undergoes elastic deformation, which is represented by the elastic strain ($\boldsymbol{\varepsilon}^{e}$). The total strain is a sum of the swelling strain, creep strain, thermal strain and elastic strain as described in equation (1). The stress-strain relationship is based on

Hooke's law (equation (2)). The material properties employed for SiC-SiC material for the current analyses are discussed in the next section.

$$\boldsymbol{\varepsilon}^{total} = \boldsymbol{\varepsilon}^{e} + \boldsymbol{\varepsilon}^{c} + \boldsymbol{\varepsilon}^{s} + \boldsymbol{\varepsilon}^{th} \quad (1)$$

$$\boldsymbol{\sigma} = \mathbf{D}\boldsymbol{\varepsilon}^{e} \quad (2)$$

2.2 MATERIAL PROPERTIES

The properties for SiC-SiC composite used in this analysis are listed in Table 1. The table also provides information about the dependence of material properties on the irradiation dose and temperature, as well as the appropriate reference citations containing the models, which have been considered in this analysis.

Table 1: SiC-SiC composite material properties for modeling channel box and their dependence on the irradiation and temperature [23].

	Temperature dependence	Effect of Irradiation
Coefficient of thermal expansion	Dependent [4]	Negligible [4]
Creep strain (Irradiation creep compliance)	Dependent [24]	Irradiation effect phenomena [24]
Swelling strain	Dependent [1, 21]	Irradiation effect phenomena [1, 21]
Specific heat capacity	Dependent	Negligible
Thermal conductivity	Dependent, basis for modeling exists [4, 21]	Strong effect, basis for modeling exists [4, 21]
Elastic constants	Dependent, basis for modeling exists [4, 21]	Minor effect, known [21]

2.2.1 SWELLING

The irradiation swelling behavior of SiC as a function of neutron fluence is shown in Figure 1. The magnitude of volumetric swelling strain increases with irradiation and saturates around one dpa. Note that the swelling is greater at lower temperature.

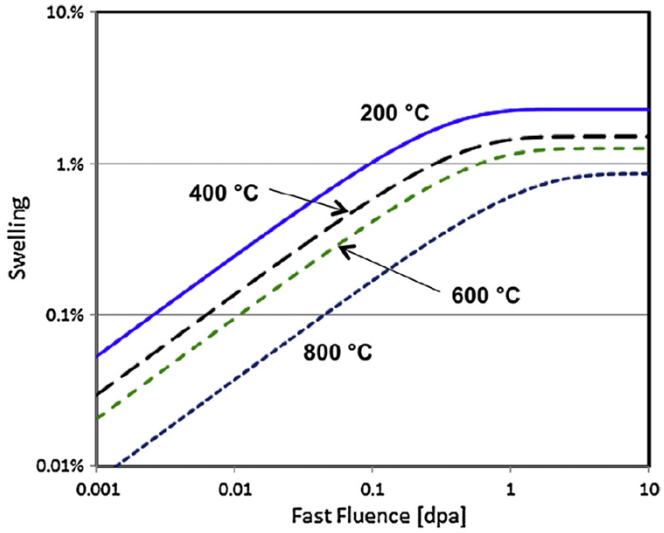

Figure 1: Volumetric swelling as a function of dose at different temperatures for CVD SiC; SiC-SiC material was assigned same swelling properties [4].

2.2.2 MECHANICAL PROPERTIES

The anisotropic elastic properties for non-irradiated SiC-SiC used in this analysis are listed in Table 2. These representative properties are based on the recently performed experimental tests for characterization of mechanical properties of nuclear grade SiC-SiC composite tubular specimens. The elastic moduli are represented by 'E', shear moduli by 'G' and Poisson's ratios by 'ν'. The subscript 'r' corresponds to the perpendicular direction of the channel box wall, the 'q' corresponds to the horizontal direction parallel to wall, and 'z' corresponds to the vertical direction.

Table 2: Elastic properties for SiC-SiC channel box [25].

E_r = 80 GPa	ν_{rq} = 0.19	G_{rq} = 70 GPa
E_q = 249 GPa	ν_{rz} = 0.20	G_{rz} = 86 GPa
E_z = 264 GPa	ν_{qz} = 0.17	G_{qz} = 110 GPa

The elastic moduli degrade with irradiation. The details about the implementation of elastic moduli degradation, and other details on the properties of SiC-SiC composite materials are available in Ref. [23, 26].

2.3 MODELING AND ANALYSIS

The thermomechanical model for the SiC-SiC channel box was set up and analyzed in both the commercial software Abaqus [20] and the fuel performance code BISON [19]. A finite element model of the channel box top section is shown in Figure 2. Figure 2 also shows the orientation of the channel box relative to the control blade. Note that the fuel assembly considered in this analysis is located near the core center; so, the flux gradients are primarily caused by the presence of water rods within a fuel assembly, in addition to the control blade positioning.

2.3.1 GEOMETRY AND MESH

The dimensions of the channel box model were representative of a channel box from the GE14 BWR, and are provided in Table 3. The model was meshed with a total of 11600 quadratic elements, with 100 elements in axial direction.

Table 3: Dimensions of the channel box considered in this analysis [27].

Geometry	Dimension
Cross-sectional width	14.02 cm
Wall thickness	3.05 mm
Height	3.71 m
Inner radius of curvature	8.0 mm
Outer radius of curvature	10.0 mm

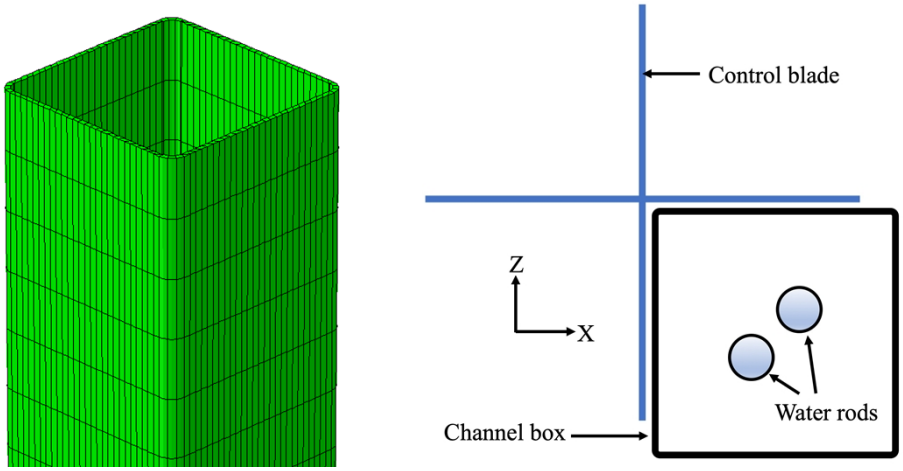

Figure 2: A section of the finite element model of channel box (left). Orientation of the channel box relative to the control blade considered in the analysis (right); the fuel assembly is considered to be located in the center of the core.

The details about the implementation of anisotropic properties, and the application of temperature and flux boundary conditions to the model are provided in Ref. [14].

2.3.2 MECHANICAL BOUNDARY CONDITIONS

In this analysis, the channel box top was allowed to freely move. It is important to note that in our prior publication [14], we have shown that when the top of the channel box is either partially or fully constrained in axial direction and rotation, stresses in the channel box rise to high magnitudes which will cause mechanical damage in the channel box [14]. Thus, mechanically constraining the top section of a SiC-SiC channel box is not considered favorable from the perspective of maintaining its structural integrity, and as such, has not been considered in the current analysis.

2.3.3 MPACT/CTF COUPLING

MPACT and CTF respectively serve as the reactor physics and sub-channel thermal hydraulics codes in CASL's Virtual Environment for Reactor Analysis Core Simulator. The computational tools have been internally coupled so that fuel and moderator temperatures and densities calculated by CTF are passed to MPACT and are used to update macroscopic cross sections. Reactor physics calculations are then performed by MPACT, and relative pin powers are passed back to CTF. This process occurs iteratively until convergence criteria are met. This fully coupled approach is expected to increase the accuracy of calculations because of the relatively large void fraction that occurs in a BWR, which plays a significant role in neutron moderation and power distribution.

The MPACT neutron transport calculations involved a 2D/1D approximation to the Boltzmann transport equation, which employs a method of characteristics algorithm in the radial direction and an SP3 method in the axial direction [28]. CTF is an updated version of the COBRA-TF legacy sub-channel code from the CASL project that uses a two-fluid, three-field approach to solving conservation equations. Both MPACT and CTF provide high-fidelity, 3D solutions on a pin-resolved scale.

2.3.4 BWR MODEL GEOMETRY AND INITIAL CONDITIONS

The neutronic thermal-hydraulic model considers the fuel assembly in order to obtain the required flux and temperature profiles. The BWR models created in MPACT/CTF are based on a 10 × 10 fuel pin lattice design, which is representative of a GE14 design [18]. The geometry of the BWR fuel assembly models used for this study is based on the geometric data detailed in the thesis by Ferroni [27], as are the power, pressure, and coolant mass flow rate. Seven axial zones were used in the computer models, each of which contains a unique fuel loading pattern [29]. These inputs match those used in Simulation 1 of the previous CTF and Serpent channel box analysis [14]. Reflective boundary conditions are used, making the models used in this study representative of assemblies near the center of the reactor core.

Thermal properties of irradiated SiC-SiC [4, 21] were implemented in the CTF input decks for either the cladding or channel box, depending on the case. In the channel box cases, heat slabs were connected to the sub-channels along the periphery of the assembly in CTF. A 47-group neutron cross-section library was used in MPACT. In the channel box study using Serpent (which uses a continuous cross-section library), a 0.1 MeV cutoff was used for tallying fast neutron flux [14]. This cutoff is not available in the 47-group library, while the nearest fast neutron cutoff energies available in the current analysis are 0.067 MeV and 0.183 MeV. Single fuel assembly models with a SiC-SiC channel box were modeled using both cutoffs to show the impact on fast flux tallies.

MPACT/CTF is capable of modeling the cruciform control blades used in BWR cores. This study provides fast neutron flux and temperature distributions in cladding and the channel box for three cases: the control blade fully withdrawn, the control blade halfway inserted, and the control blade fully inserted. The control blade design implemented in the models is provided by Gauld [30]. Figure 3 shows a 2-D cross-sectional view of the single BWR assembly model used for this study and includes the control blade. Different colored fuel pins within the figure indicate different levels of U-235 enrichment. For demonstration purposes, the same power is used for all the three cases of control blade position in the fuel assembly.

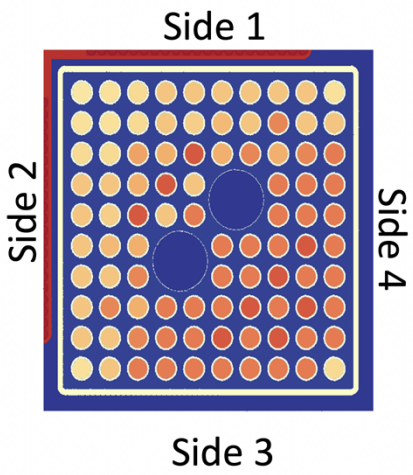

Figure 3: Cross section of the single fuel assembly model with the control blade (shown in red on sides 1 and 2) fully inserted.

3. RESULTS

3.1 SINGLE FUEL ASSEMBLY NEUTRONIC AND THERMAL HYDRAULIC RESULTS

3.1.1 SIC-SIC FUEL ROD CLADDING

Figure 4 shows the fast neutron flux distribution within a vertical slice of the fuel assembly model for the control blade fully withdrawn, halfway inserted, and fully inserted, respectively, using the 0.067 MeV cutoff for defining the fast neutron flux. The figure indicates a significant axial and radial gradient in the fast flux and that the location of the maximum flux changes depending on the control blade insertion position.

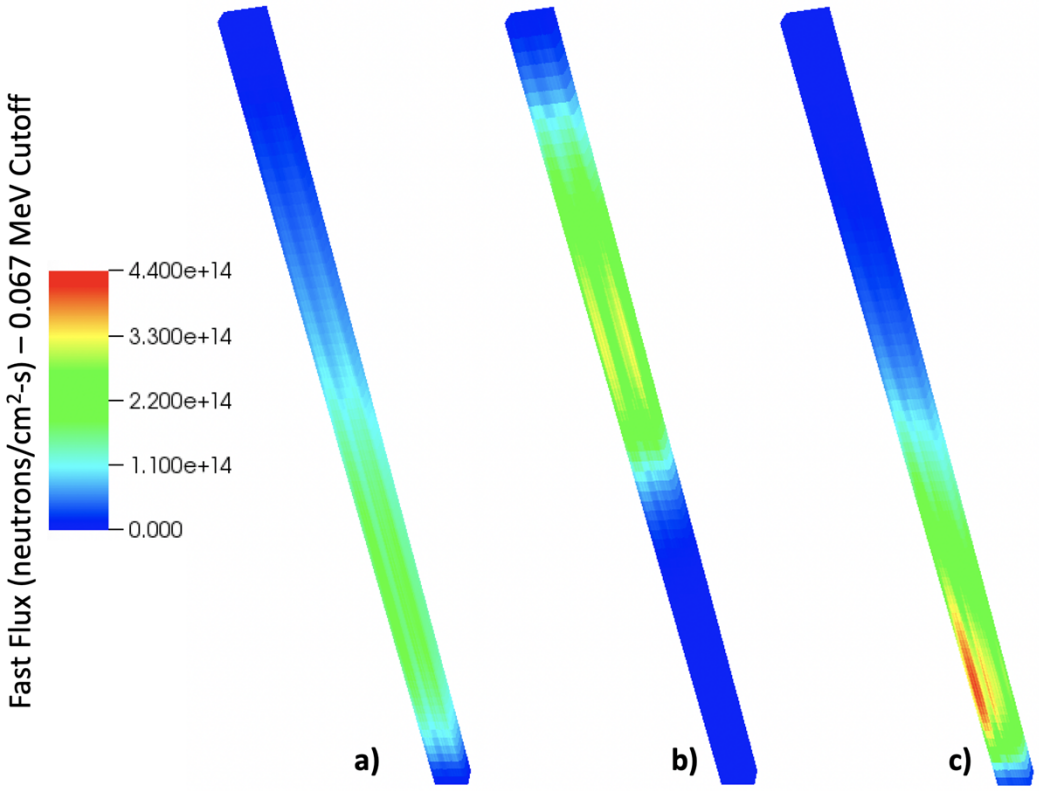

Figure 4: Fast flux distribution in the center of a BWR fuel assembly when the control blade is (a) fully withdrawn, (b) halfway inserted, and (c) fully inserted.

Figure 5 shows a 2-D cross section from a portion of the fuel assembly at the location of the maximum fast flux in the case of the fully withdrawn control blade. The radial and azimuthal gradient in fast flux is clearly evident in the figure, but was not taken into account in the previous SiC-SiC cladding deformation study [14]. A zoomed-in portion of a quadrant of a pin cell is shown for better clarity of the mesh regions and demonstrates flux gradients with a maximum gradient of about 2-9 % in the azimuthal direction. The higher gradients occur in the fuel rods near the assembly edge, near the water rods and near the control blade.

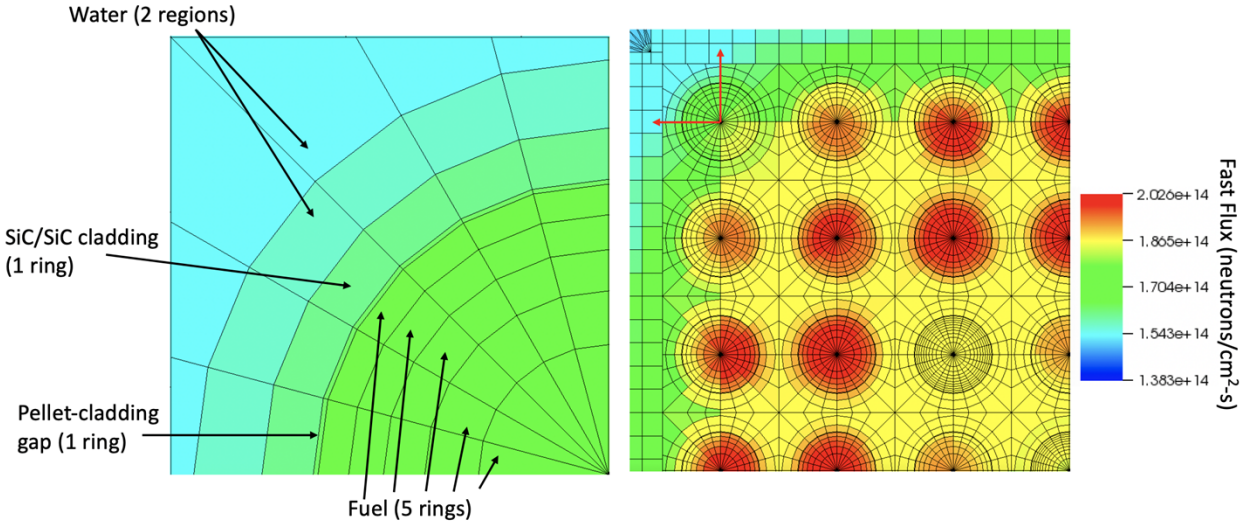

Figure 5: Two-dimensional cross section of a BWR fuel assembly showing fast flux gradient.

Figure 6 shows the maximum cladding inner surface temperatures for each fuel pin in the fuel assembly for the three control blade cases. As with the fast flux, there is significant axial and radial variation in cladding temperatures, and the location of the maximum temperature is dependent upon the control blade position. For the fully withdrawn control blade case, the maximum cladding inner surface temperature occurring in the model is 424.6°C. CTF results show that the maximum cladding outer surface temperature occurring in the model is 297.6°C, which shows the magnitude of radial temperature gradients occurring in the cladding. Although the previous SiC-SiC fuel rod deformation analysis consisted of a single fuel rod, the results shown here imply that the deformation would be a function of the rod's position within a fuel assembly and that each rod within a fuel assembly might experience a different magnitude of deformation.

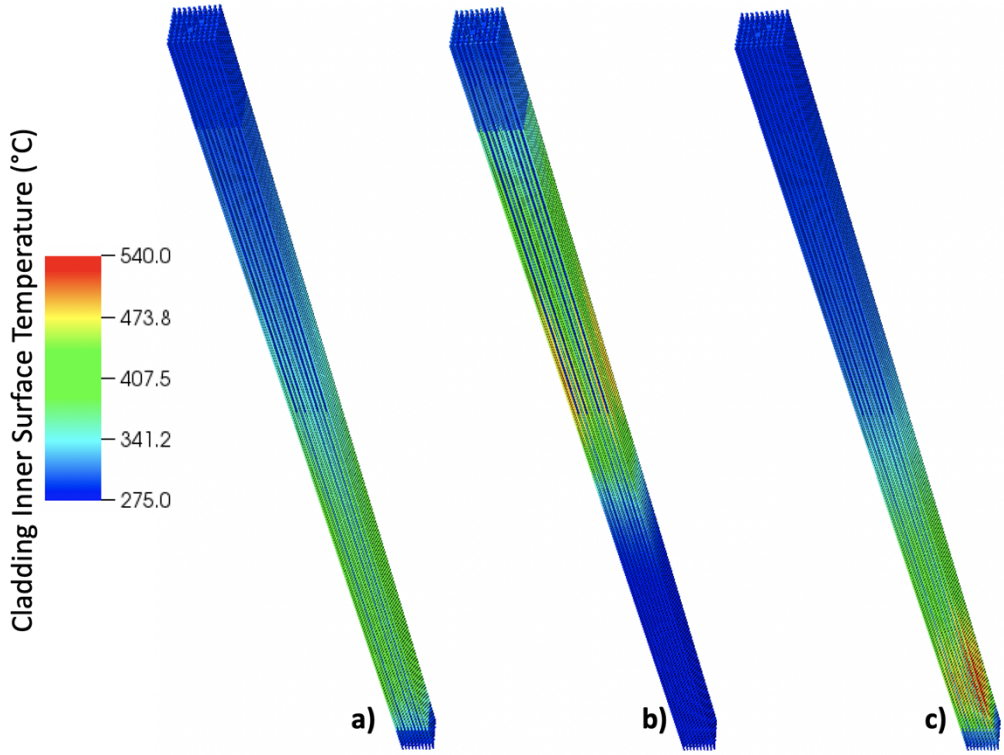

Figure 6: Cladding inner surface temperature distributions when the control blade is (a) fully withdrawn, (b) halfway inserted, and (c) fully inserted.

3.1.2 SIC-SIC CHANNEL BOX

Figure 7 through Figure 9 show the 3D spatial distribution of the fast neutron flux in a BWR channel box for the fully withdrawn control blade, the partially inserted control blade and the fully inserted control blade positioning, respectively. The distributions using the 0.067 MeV and 0.183 MeV neutron energy cutoffs are both shown, as is the percent difference between using these two different energy cutoff values. The difference in fast flux between the two cutoffs is spatially dependent and ranges from approximately 4% to 17%, depending on the control blade position. All four sides of the channel box are shown for a clear visualization of the radial heterogeneity in the flux distributions. The side numbers correspond to those shown in Figure 3. Figure 10 through Figure 12 show the temperature distributions in the channel box for the fully withdrawn, partially inserted, and fully inserted control blade positions, respectively.

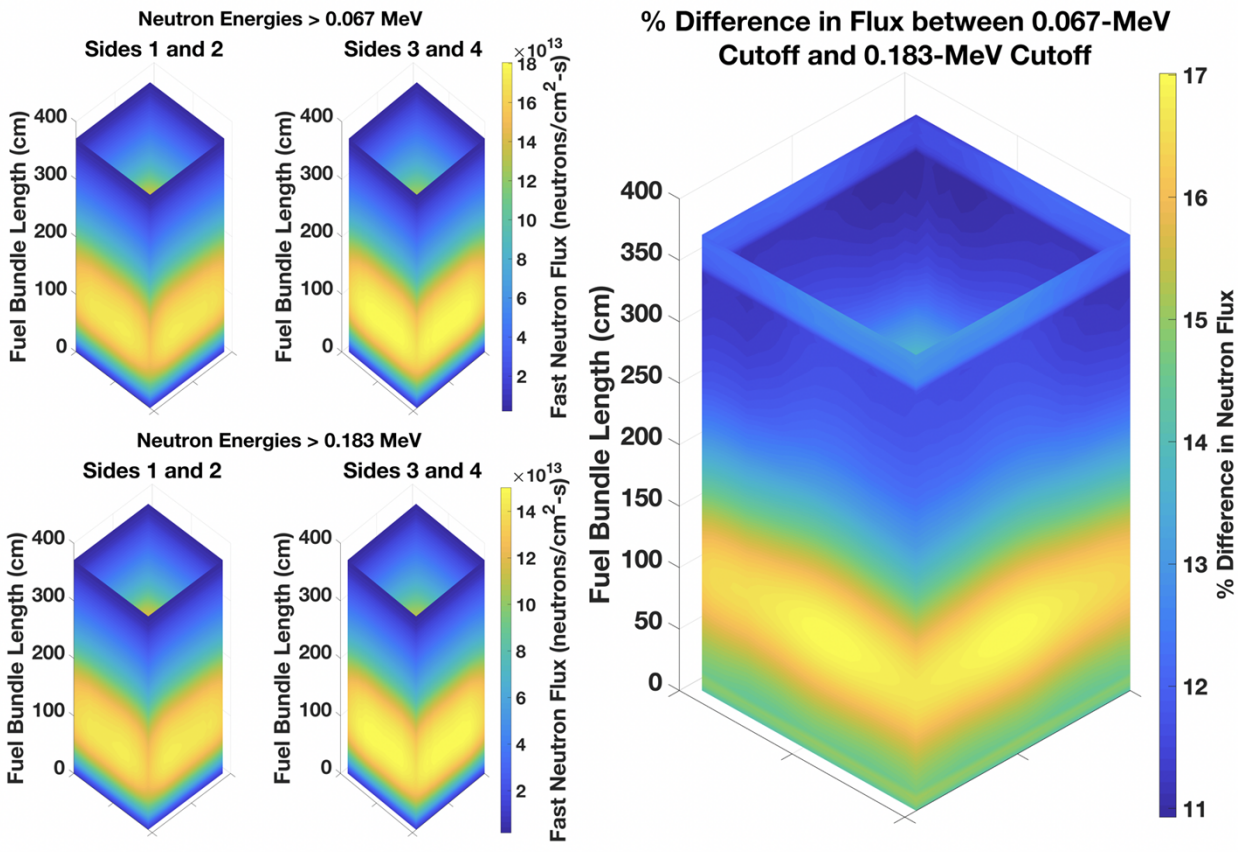

Figure 7: Fast neutron flux distribution in a SiC-SiC channel box using a 0.067 MeV cutoff (top), 0.183 MeV cutoff (bottom), and the percent difference in flux between the two cutoffs (right) with the control blade fully withdrawn.

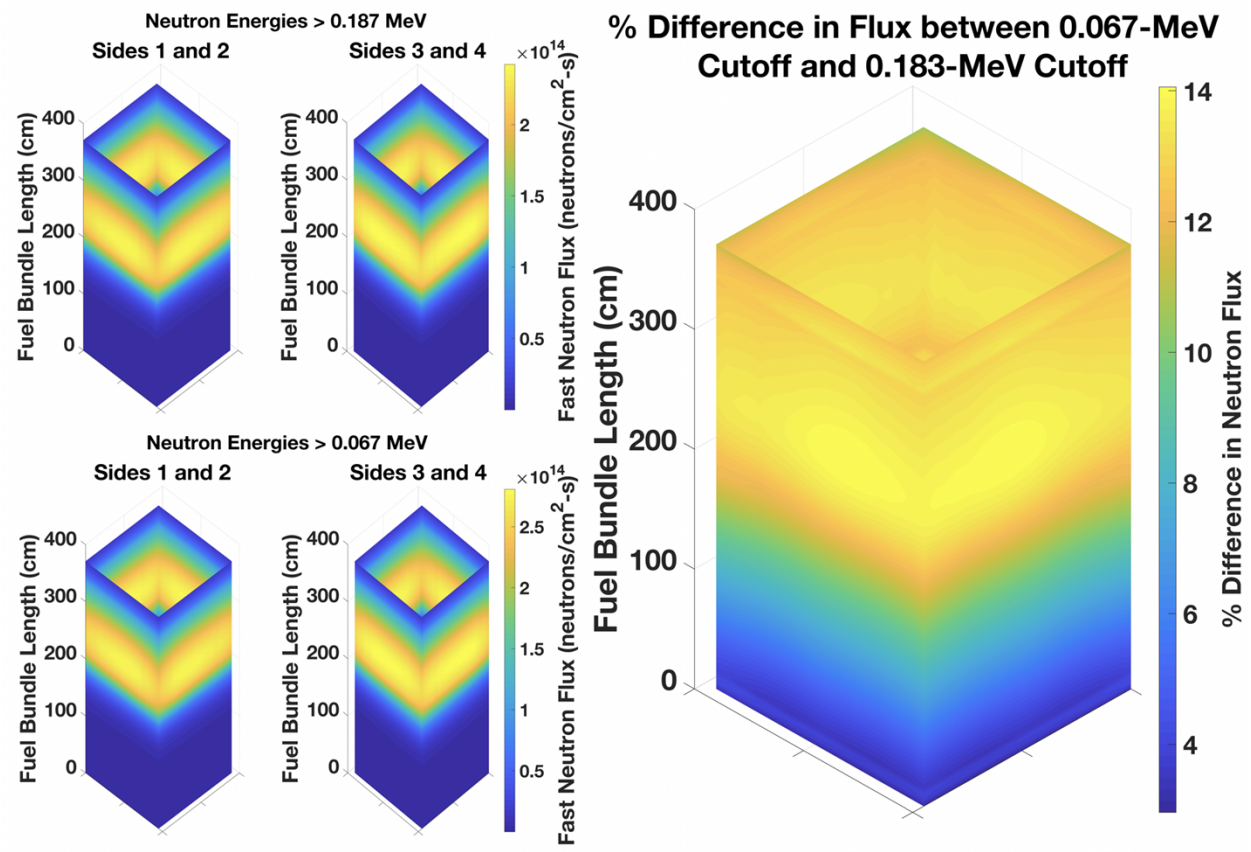

Figure 8: Fast neutron flux distribution in a SiC-SiC channel box using a 0.067 MeV cutoff (top), 0.183 MeV cutoff (bottom), and the percent difference in flux between the two cutoffs (right) with the control blade halfway inserted.

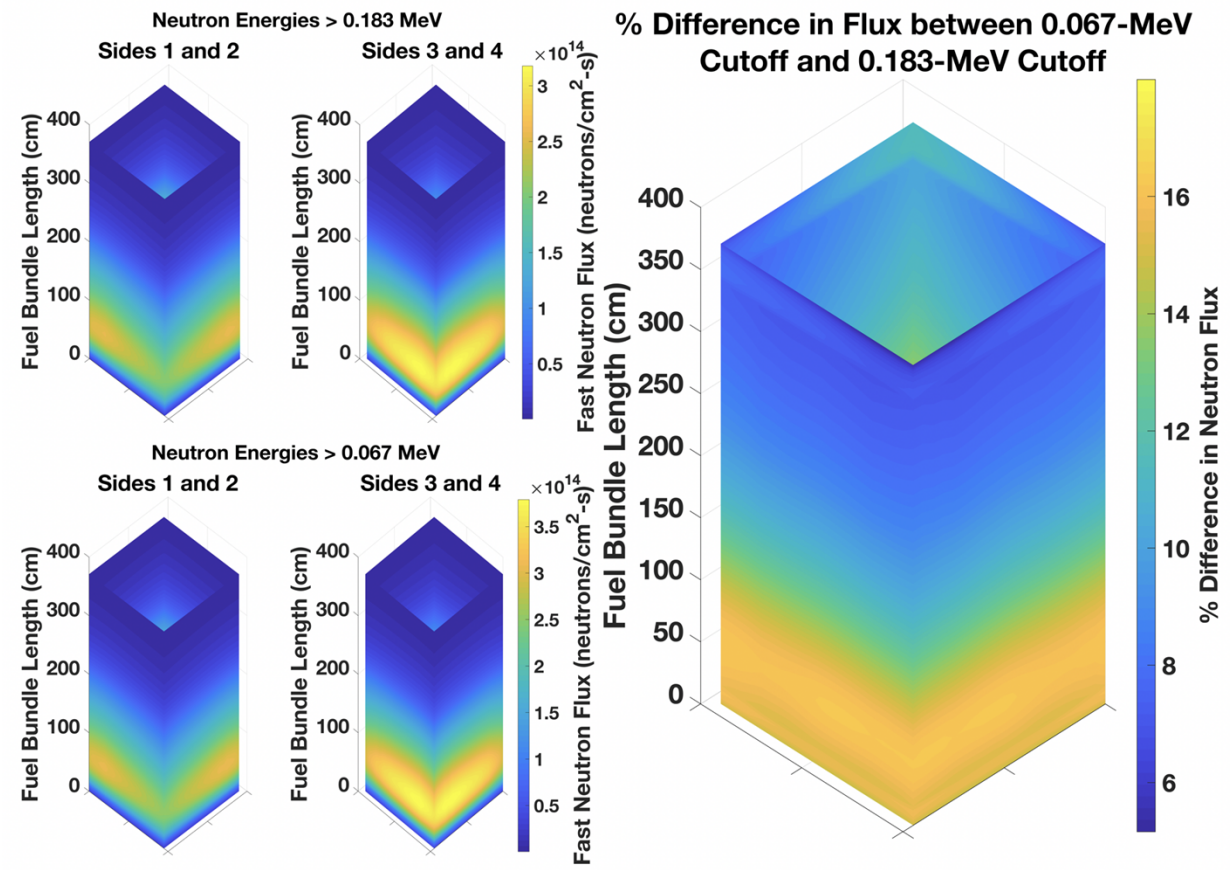

Figure 9: Fast neutron flux distribution in a SiC-SiC channel box using a 0.067 MeV cutoff (top), 0.183 MeV cutoff (bottom), and the percent difference in flux between the two cutoffs (right) with the control blade fully inserted.

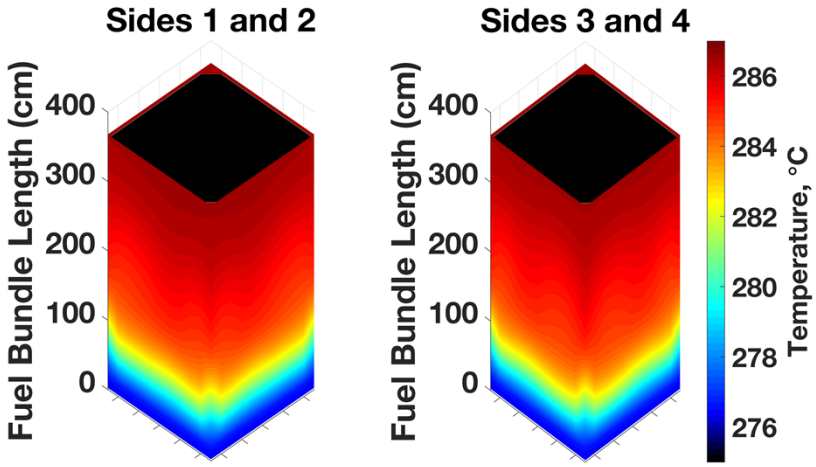

Figure 10: Temperature distribution in the channel box for the case with control blade fully withdrawn.

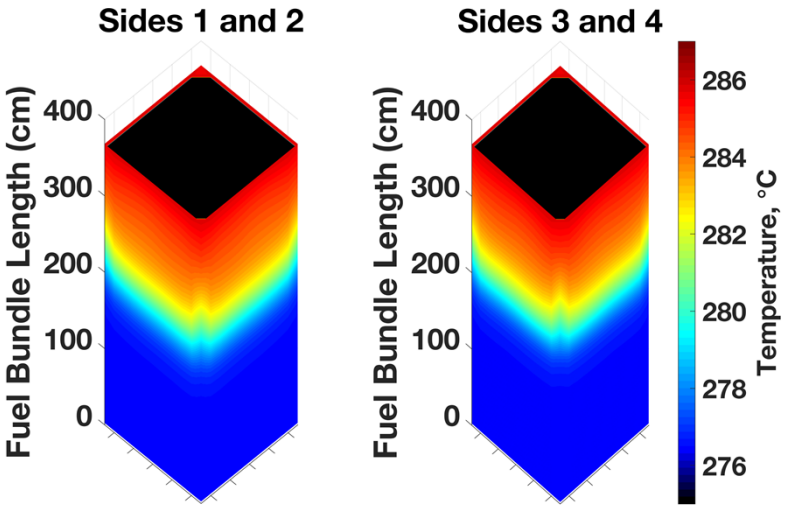

Figure 11: Temperature distribution in the channel box for the case with control blade halfway inserted.

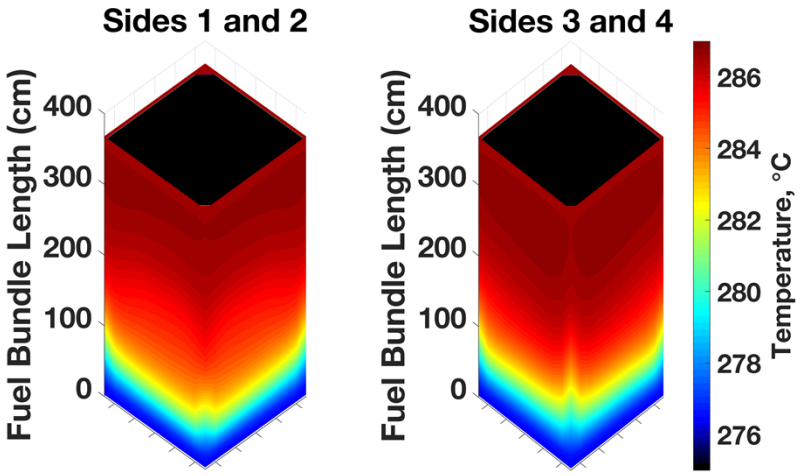

Figure 12: Temperature distribution in the channel box for the case with control blade fully inserted.

Figure 7 through Figure 12 show that there is significant axial variation in the fast flux and temperature, regardless of the control blade position. The axial gradient is most pronounced when the control blade is partially inserted, since this position causes a top-heavy power shape in the fuel assembly. The radial gradient in fast flux and temperature becomes most pronounced when the control blade is fully inserted because the power is most depressed along the two sides of the assembly adjacent to the control blade wings. Linearly interpolating between the maximum flux values calculated using the two different neutron energy cutoffs (1.804×10^{14} neutrons/cm^2-s for the 0.067 MeV cutoff and 1.502×10^{14} neutrons/cm^2-s for the 0.183 MeV cutoff) gives an estimate of the flux at a 0.1 MeV neutron energy cutoff of 1.644×10^{14} neutrons/cm^2-s. This value is approximately 25% less than the peak fast flux calculated in our previous work using CTF and Serpent [14]. The difference in peak flux values is caused by using a 3D method with pin-resolved thermal hydraulic feedback in this study versus a 2D method using interpolation and averaged thermal hydraulic parameters in the previous study.

3.2 LATERAL DISPLACEMENT

The structural analysis for the SiC-SiC channel box was performed for three different positions of the control blade with respect to the fuel assembly: 1) Case W: control blade fully withdrawn 2) Case H: control blade inserted halfway and 3) Case F: control blade fully inserted. The analysis was performed using the commercial finite element software Abaqus as well as the fuel performance code BISON. The results presented in this section are based on the energy cutoff of 0.067 MeV for calculating the fast neutron flux from total neutron flux. The sensitivity of the results to the energy cutoff value is subsequently discussed in section 3.3.

3.2.1 CASE W: CONTROL BLADE FULLY WITHDRAWN

Figure 13 shows the contour plots of displacement in the z-direction (perpendicular to wall) for case W with the control blade fully withdrawn. The total lateral displacement of the channel box with time for this control blade position is shown in Figure 14.

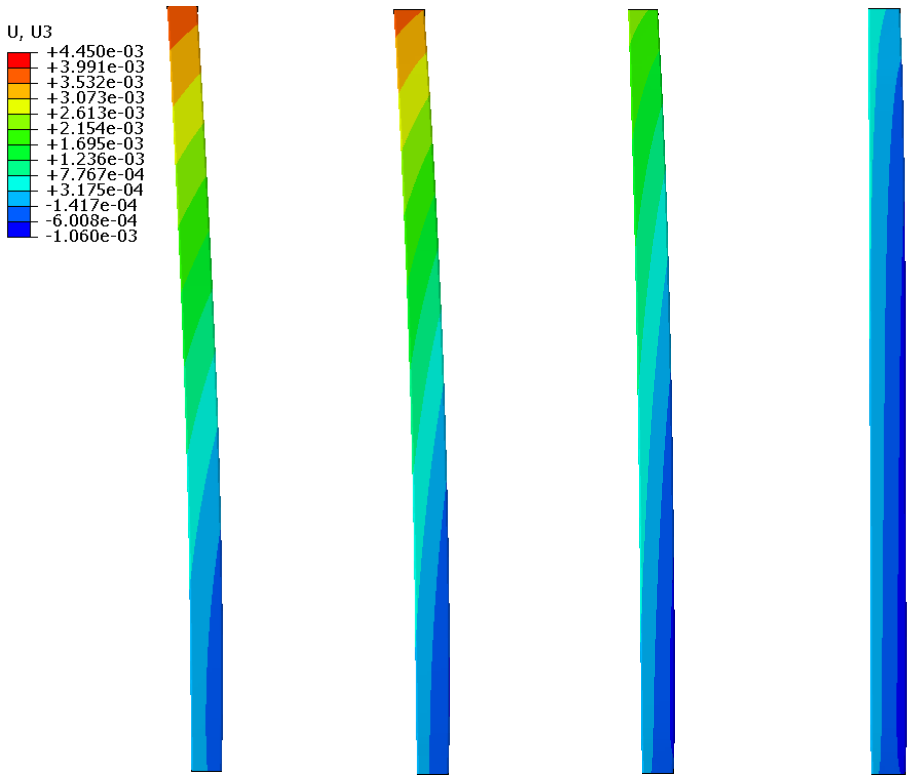

Figure 13: Lateral displacement (units: meter) of the channel box along the z-direction (perpendicular to wall) after 11 days, one month, two months and four months (from left to right) for case W. Displacement is exaggerated for visualization purpose. The total displacement is shown in Figure 14.

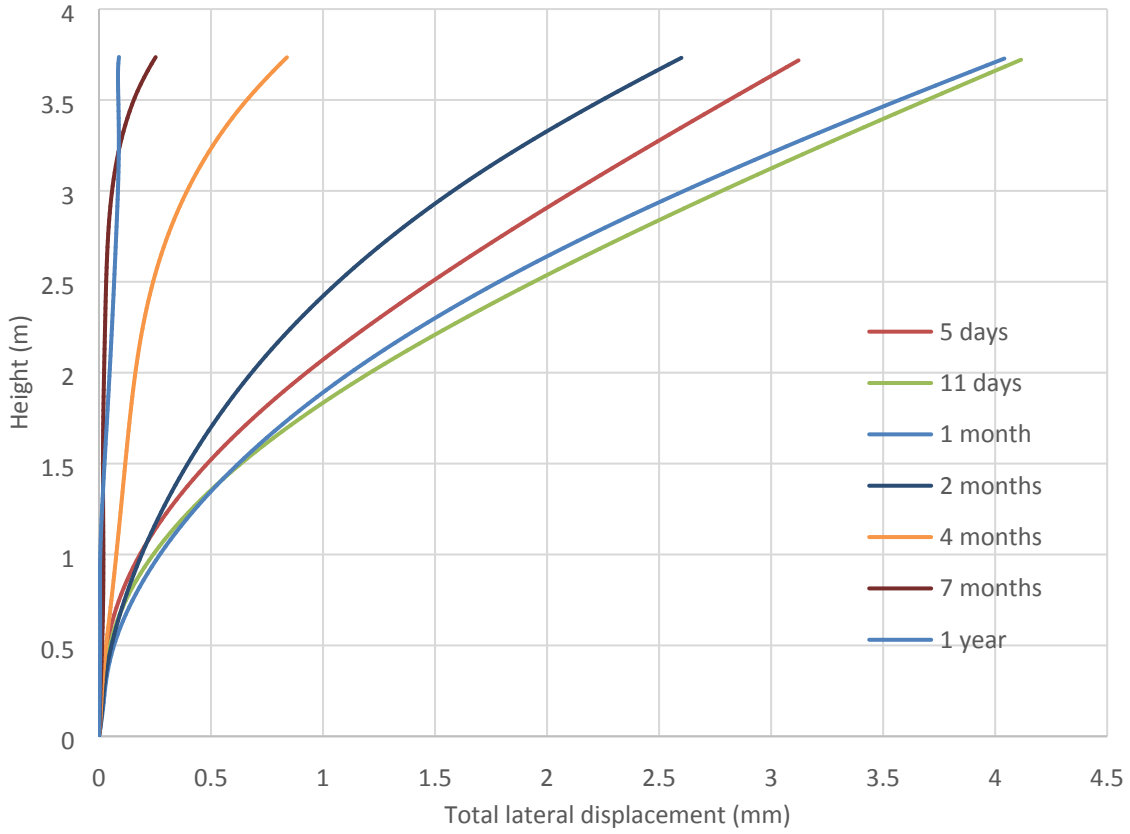

Figure 14: Total lateral displacement versus channel box height at different operating times for the case of control blade withdrawn (cut-off energy E_{cutoff} = 0.067 MeV). Note that total lateral displacement is composed of lateral displacements in x and z directions.

Figure 14 shows that the total lateral displacement initially increases with time, reaching a maximum magnitude after about 11 days, and then decreases gradually with increasing time. As discussed in Ref. [23], irradiation induced swelling is the dominating mechanism for SiC-SiC material deformation in comparison to thermal expansion and creep. The neutron flux gradient across the width of the channel box, as shown in figure 7, is significant (~9%) and causes differential swelling in the channel box. This swelling gradient across the width of the channel box causes the channel box to bend laterally. The temperature gradient across the channel box width is insignificant, as shown in figure 10.

As the swelling and swelling gradient increases with time, the bending magnitude also increases. When the irradiation induced swelling begins to saturate, the swelling gradient across the channel box width decreases, and consequently, the lateral bending also decreases causing the channel box to straighten. However, it is important to note that even after a year of in-core operation, when the swelling in the entire channel box has saturated, a residual displacement of ~0.1mm remains in the channel box. This residual displacement is due to differential saturated-swelling caused by the relatively small temperature gradient of about ~2-3 °C across the width of the channel box.

There is a small difference in the displacement results presented here and those previously published for a case of fully withdrawn control blade [14]. These differences are result from the different codes used in the neutronics analysis. In the earlier analysis, Serpent was used to calculate the fast flux, and those calculations

did not incorporate the temperature feedback from the CTF code. The present analysis uses MPACT for neutronics analysis and incorporates a thermal-hydraulic feedback; hence, we believe the results presented here are more accurate compared to the methodology that was used previously. Figure 15 shows the stress distribution in the channel box. The maximum stress was found to be 65 MPa which is below the proportional limit of the material ~90 MPa, hence no microcracking is expected.

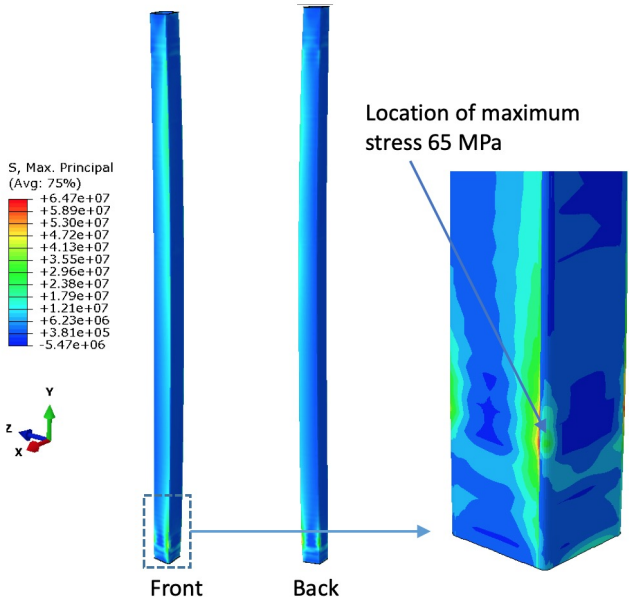

Figure 15: Maximum principal stress distribution in the channel box for the case with control blade withdrawn (E_{cutoff} = 0.067 MeV). Units of stress: Pa. Maximum stress of 65 MPa reached after 46 days.

3.2.2 CASE H: CONTROL BLADE INSERTED HALFWAY

For case H, the channel box undergoes lateral bending which continuously increases with time until about 2 years of in-core operation, beyond which there insignificant further bending of the channel box, as shown in Figure 16. Note that the bending rate decreases with time. The fast neutron flux gradient is about 34% across the width of the channel box for this case. The maximum lateral displacement at the top of the channel box is about 6.2 mm.

Since the control blade is inserted halfway from the bottom towards the top, the lower half region of the channel box receives much less neutron flux compared to the upper half (see Figure 8). This leads to less swelling in the lower region of the channel box than in the upper region. Since the swelling in the lower region does not saturate, the swelling as well the differential swelling continues to increase with time up to two years, leading to continuously increased bending in the lower half of the channel box. The swelling in the upper region of the channel box, unlike that in the lower region, saturates early on during the reactor cycle leading to straightening in the upper region. The net effect is that the channel box top does not undergo further lateral displacement and stays at almost the same position after 2 years.

Figure 17 shows the maximum principal stress distribution in the channel box, and shows that a maximum stress of 125 MPa will develop in the channel box after about 141 days. Since the stress is greater than the proportional limit stress of the material (~90 MPa [31]), matrix microcracking is likely to occur.

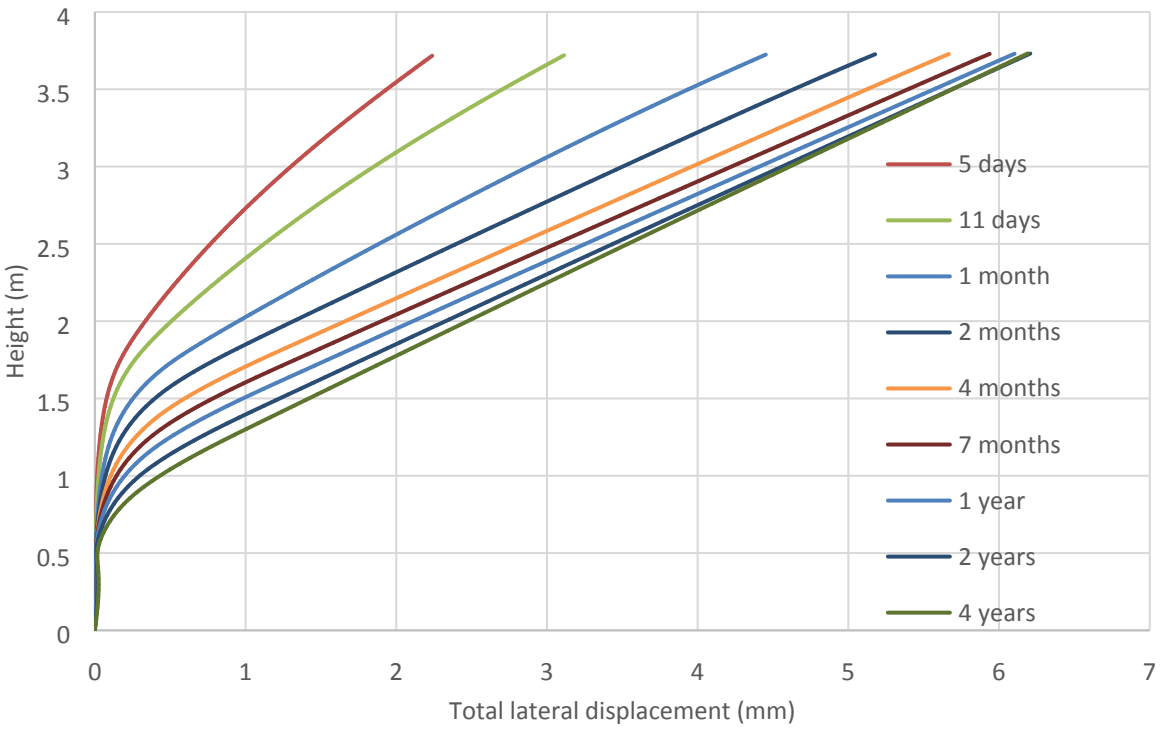

Figure 16: Total lateral displacement versus channel box height at different operating times for the case of control blade inserted halfway and E_{cutoff} = 0.067 MeV.

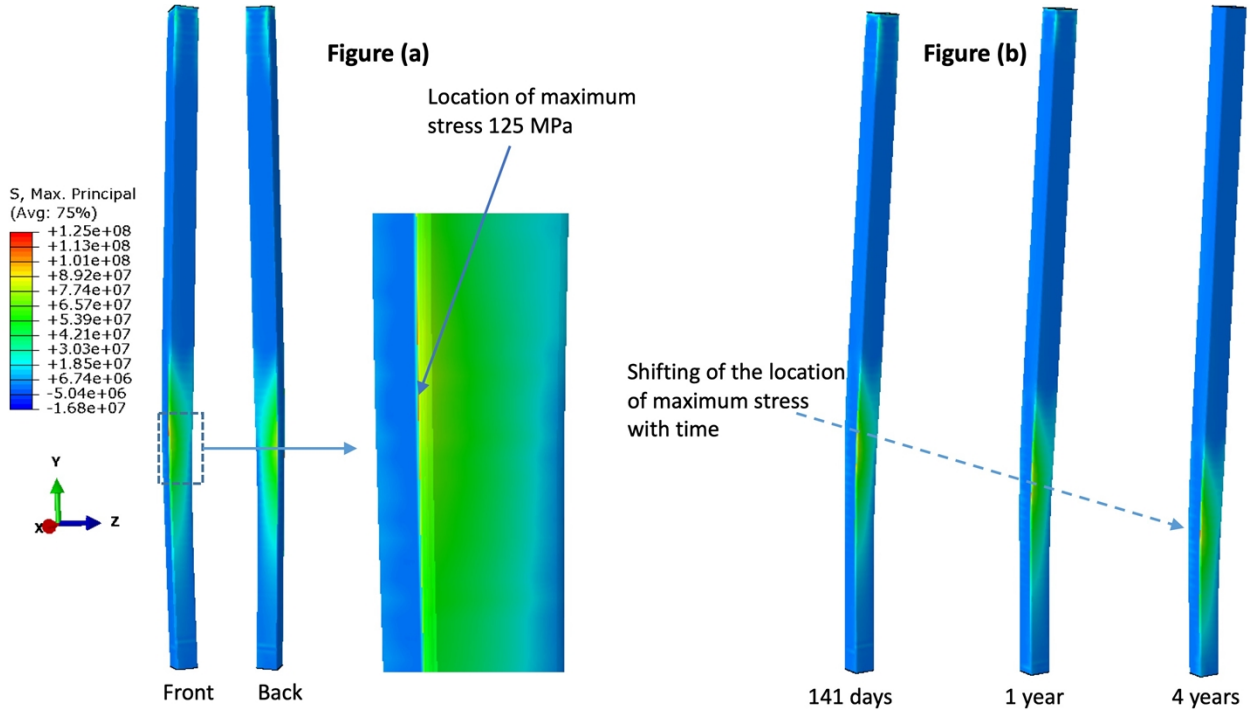

Figure 17: Maximum principal stress distribution in the channel box for the case with control blade inserted halfway into the assembly (E_{cutoff} = 0.067 MeV). Units of stress: Pa. Maximum stress of 125 MPa reached after 141 days.

3.2.3 CASE F: CONTROL BLADE FULLY INSERTED

For the case F in which the control blade is fully inserted, the channel box bending behavior is similar to that for case W. As shown in Figure 18, the channel box undergoes significant lateral bending initially, followed by gradual straightening. This similar bending behavior can be attributed to the similar neutron flux distribution in the channel box in the axial direction for these two control blade positions: higher flux in the lower half region of the channel box which decreases towards the top (see figures 7 and 9). However, for this case F, the maximum total lateral displacement is significantly higher as the top of the channel box undergoes a maximum total lateral displacement of about 14.4 mm. The greater lateral displacement compared to case W can be attributed to the larger gradient in fast neutron flux (~36%). The position of maximum displacement is reached after about 11 days. Although the fast neutron flux gradient across the channel box width for this case (~36%) is about same as for the case H (~34%), the different axial distribution of neutron flux leads to very different magnitudes of maximum lateral bowing (14.4 mm vs. 6.2 mm).

Figure 19 shows the distribution of maximum principal stress in the channel box. It was found that a maximum stress of 155 MPa was reached after 17 days. Since the stress is greater than the proportional limit stress of the material (~90 MPa), matrix microcracking is expected.

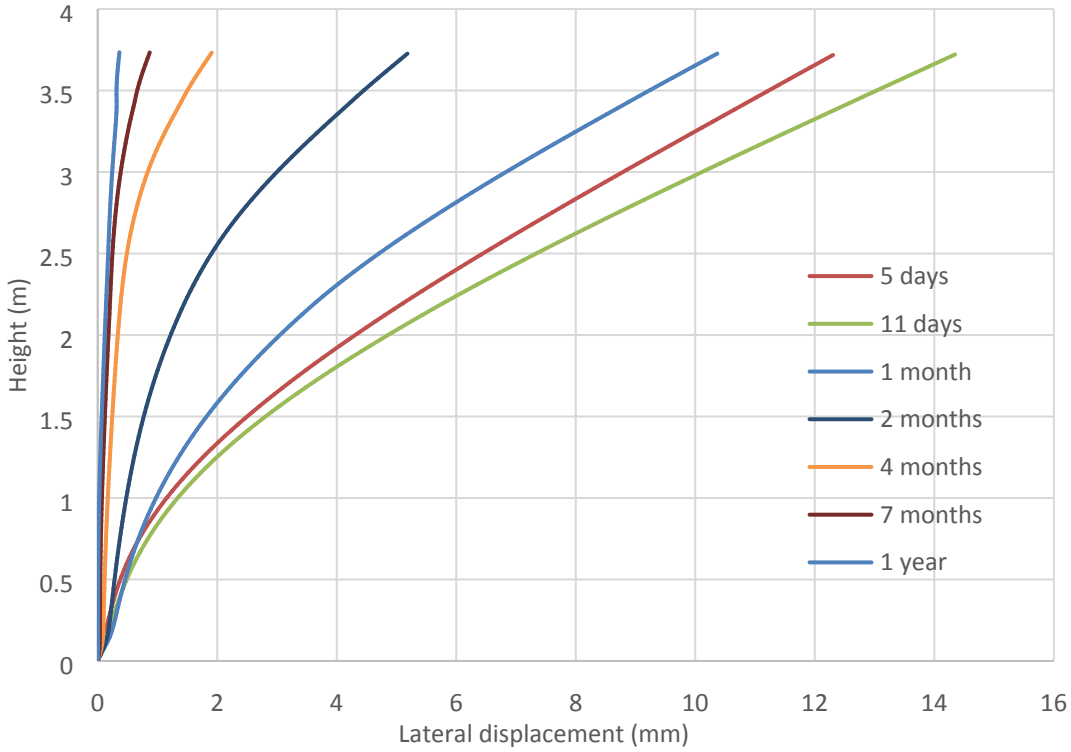

Figure 18: Total lateral displacement (in the diagonal direction) versus channel box height at different operating times for the case of control blade fully inserted and with E_{cutoff} = 0.067 MeV.

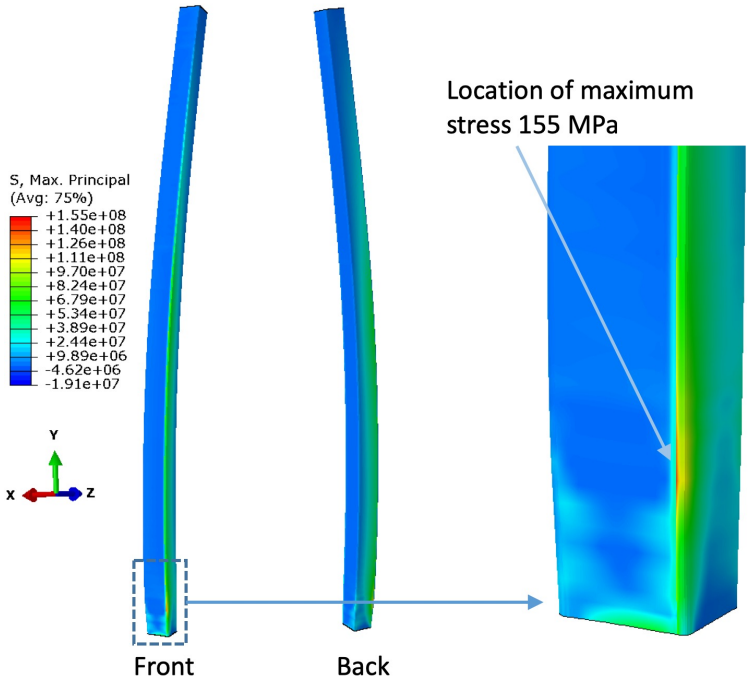

Figure 19: Maximum principal stress distribution in the channel box for the case with control blade inserted fully (E_{cutoff} = 0.067 MeV). Units of stress: Pa. Maximum stress of 155 MPa reached after 17 days.

3.3 SENSITIVITY TO ENERGY CUTOFF VALUES

The fast neutron induced displacement damage in SiC is the cause of the swelling. The fast neutron flux is calculated from the total neutron flux using an energy cutoff value, which is selected subjectively. Since the selected energy cutoff determines the fast flux, and ultimately the resultant deformation in the channel box, a study was performed to understand the sensitivity of channel box displacement (bending) to the chosen energy cutoff. In this study, two energy cutoff values were used: 0.067 MeV and 0.183 MeV. Figure 20 plots the total lateral displacement for these two energy cutoffs for the case of a fully inserted control blade.

It can be noted that changing the energy cutoff for calculating fast neutron flux from total neutron flux produces a small difference in the bending magnitudes. The channel box undergoes slightly larger lateral displacement for the fast flux with energy cutoff 0.183 MeV than that for the fast flux with energy cutoff 0.067 MeV during the entire time history for cases H and F, and during 1-5 months for case W. This larger lateral displacement for the fast flux with energy cutoff 0.183 MeV is due to the sharper gradient in the fast flux across the channel box width. Figure 21 shows the variation of total lateral displacement with time, and demonstrates that while there are minor differences in the magnitude of the displacement, the time dependence is essentially independent of the fast neutron energy cutoff used in the analysis.

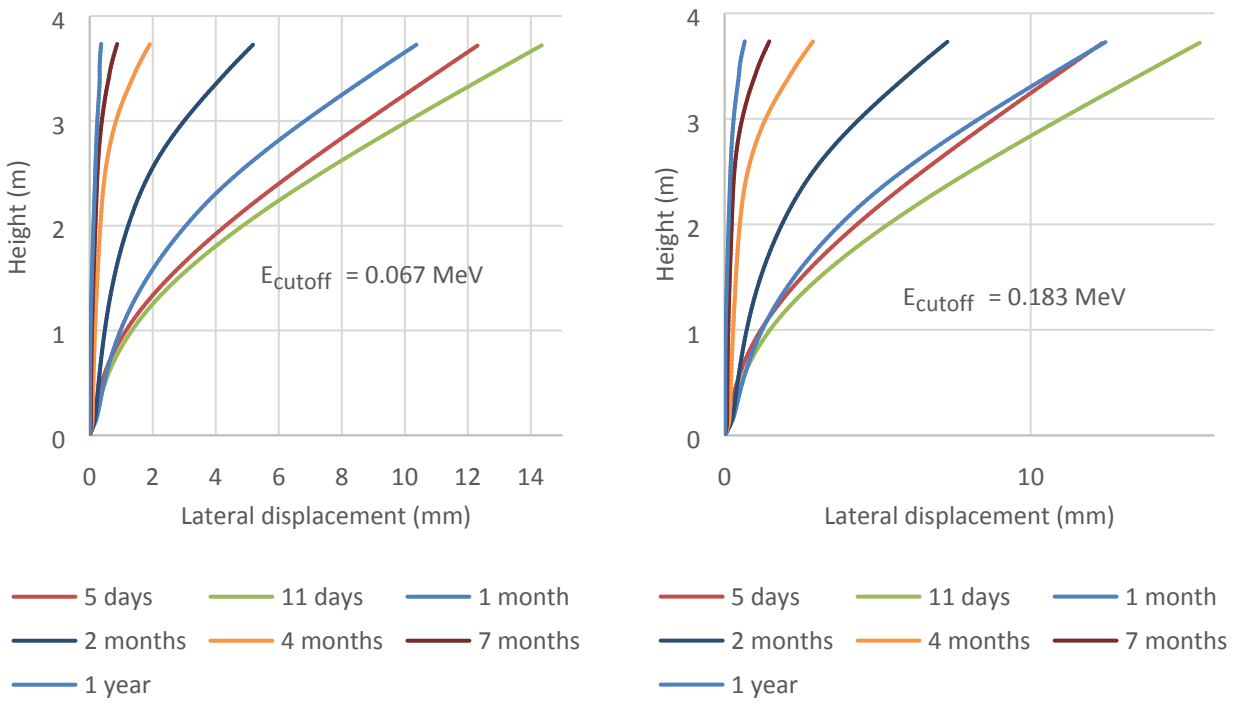

Figure 20: Plots of the total lateral displacement magnitudes for the two neutron energy energy cutoffs (0.067 MeV and 0.183 MeV) at different times for the case of a fully inserted control blade.

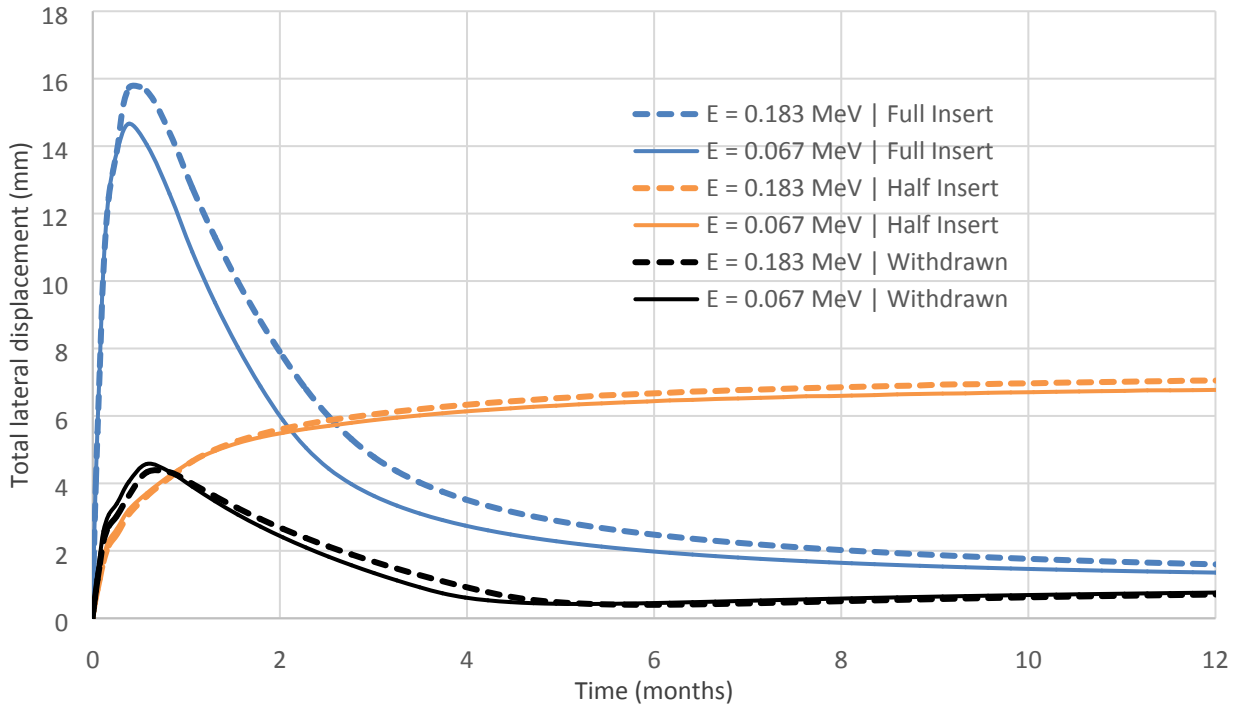

Figure 21: Comparison of the total lateral displacement at the top of the channel box as a function of time and fast neutron energy energy cutoff at different times for the three different control blade positions.

3.4 COMPARISON BETWEEN ABAQUS AND BISON RESULTS

The displacement analyses were performed using two different codes: the commercial finite element analysis code Abaqus and the fuel performance code BISON, to provide a benchmark of the codes against each other. Table 5 shows a comparison of the maximum displacements obtained from each finite element analysis code. The predictions are in good agreement with each other, as the difference in the maximum displacement is less than half a millimeter. The displacement evolution trend predicted by the codes was also found to be in good agreement (see Figure 22).

Table 4: Comparison of maximum total lateral displacements obtained from the Abaqus software and BISON code for the three control blade positions.

	Maximum total lateral displacement (mm)		
Case	**Abaqus solution**	**Bison solution**	**Difference**
W: Control blade withdrawn	4.1	3.8	0.3
H: Control blade half-inserted	6.2	6.2	0.0
F: Control blade full-inserted	14.4	14.0	0.4

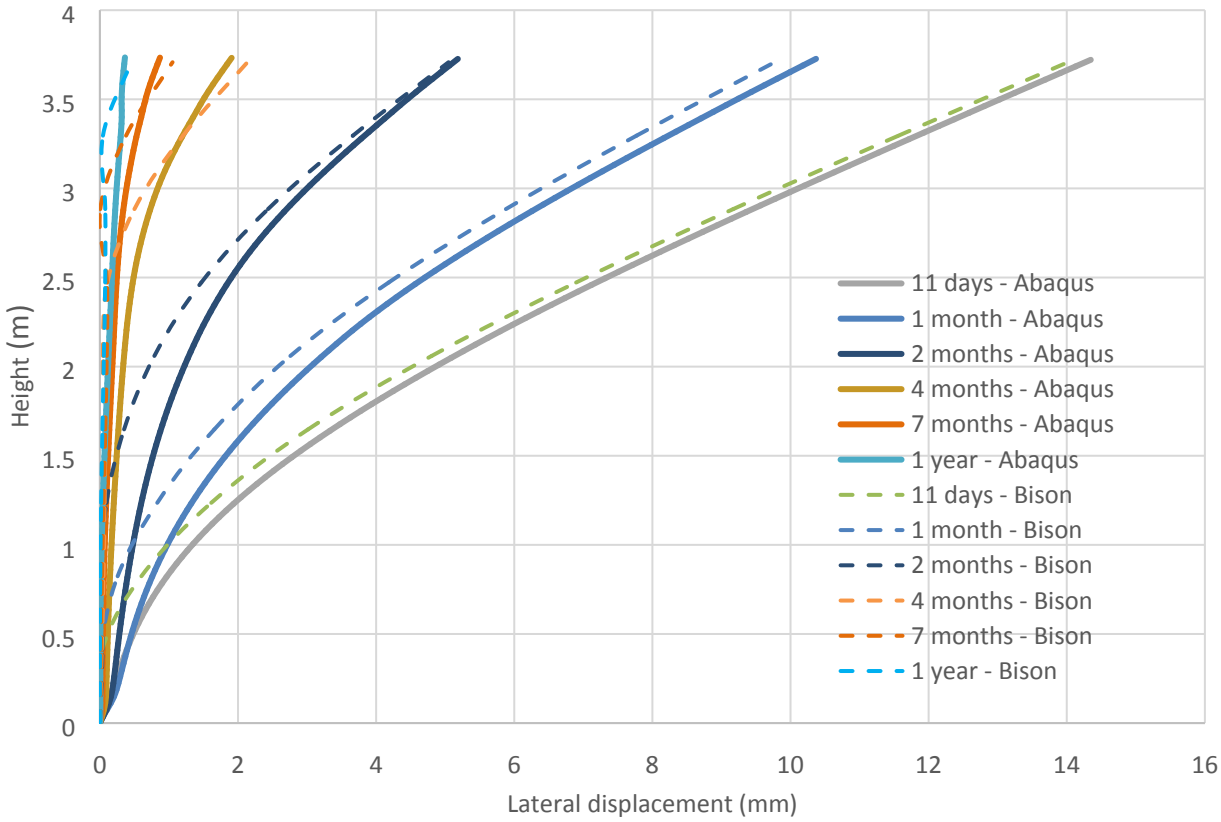

Figure 22: Comparison of the time dependent lateral displacement predicted by BISON (dashed lines) and Abaqus (solid lines) as a function fo time, for the fully inserted control blade (E_{cutoff} = 0.067 MeV).

4. DISCUSSION

The movement of the control blade controls the reactivity. Thus, a smooth movement of the control blade is essential for reactor operation and safety. As shown in the previous section, the channel box may undergo lateral bending due to irradiation induced material swelling that depend on neutron flux, fluence and temperature. This lateral bending may cause interference between the channel box and control blade, and inhibit the movement of the control blade through the fuel assembly. The next obvious question is how much interference may occur due to this bending of the channel box, and how severe such interference would be.

In this context, Cantonwine et al. performed studies on the effect of interference on control blade movement in several General Electric (GE) plants [32, 33]. In those studies, the interference between the control blade and the channel box was quantified using two parameters: Channel Interference Metric (CIM_{cell}) and Half-Gap Channel Interference Metric ($HGCIM_{cell}$). The $HGCIM_{cell}$ parameter is shown in Figure 23; for detailed description see Ref. [34]. The severity of the interference was quantified based on the 'settle time'. The settle time is defined as the time it takes for the control blade to move from one notch position to another notch position. A normally moving control blade without any interference has a settle time of two seconds or less; a settle time of more than two seconds indicates the possibility of mild interference – this situation

is call ‘slow settle’, and a settle time of more than 30 seconds indicates a severe interference – this situation is called ‘no-settle’. The studies by Cantonwine et al. [32, 33] revealed that the CIM_{cell} of less than 0.5 mm correlate to normal or near normal settling times; CIM_{cell} in range 0.5 – 1.0 mm correlated to slow or no-settle conditions, and CIM_{cell} greater than 1.0 mm correlated to no-settle condition; $HGCIM_{cell}$ greater than 5.0 mm correlated to slow or no-settle condition.

The maximum displacements at the top section of the channel box, calculated in this study for the three cases of control blade position are listed in Table 6. Table 6 also lists the corresponding $HGCIM_{cell}$ for three different widths of initial gap. Note that the initial gap can vary based on design and manufacturing. Based on the Cantonwine et al. studies, slow-settle or no-settle condition is expected when $HGCIM_{cell}$ is greater than 5.0 mm. Table 6 is color coded such that simulation predictions that would correspond to slow or no settle condition are shown in red.

For the control blade fully withdrawn (case W), interference between the channel box and control blade is not expected for any of the initial gap widths considered. GE-BWRs have half gaps of about 3 mm (S-Lattice), 4.2 mm (C-Lattice) and 4.9 mm (D-Lattice) [33]. However, for the case with the control blade inserted halfway (case H), interference is expected for the half gap widths of 3.0 mm and 4.2 mm leading to either slow or no settle condition, although for an initial half gap width of 4.9 mm interference is not expected. Finally, for the fully inserted control blade position (case F), interference is expected for all the initial half gap widths considered here, and either slow or no settle of the control blade is expected. In summary, the more the control blade is inserted, the greater is the lateral deflection and higher is the possibility of interference of the control blade with the channel box. Note that during reactor operation, the control blade position is dynamically adjusted, but the results presented here only considered static control blade positions that were either fully withdrawn, half inserted or fully inserted throughout the reactor operation. It should also be noted that the neutronics and thermal hydraulics results were obtained for the undeformed channel box. However, due to deformation of channel box during operation will lead to some changes in these results for fluence and temperature. Hence, the scenario for realistic control blade movement histories will differ. However, these results provide a strong indication that the channel box–control blade interference problems are likely to occur with a SiC-SiC channel box fuel assembly for smaller initial gap widths between the control blade and channel box.

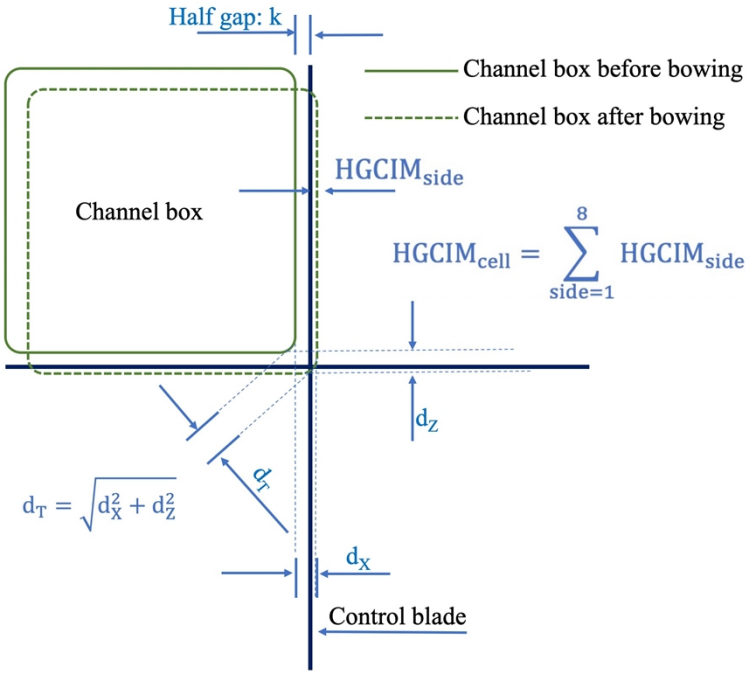

Figure 23: Simplified schematic with top view showing the bowing direction and magnitude for a channel box. d_T is the total lateral displacement.

Table 5: Half gap channel interference metric ($HGCIM_{cell}$) calculated for the channel box under different conditions of initial gap and control blade position. Cells colored red indicate slow or no-settle condition for the control blade (mild to severe interference b/w control blade and channel box). Negative sign indicates displacement in opposite direction of the coordinates axes. See Figure 2 for coordinate axes.

Case	Top displacement (mm) (X-direction)	Top displacement (mm) (Z-direction)	$HGCIM_{Cell}$		
			Initial gap 3.0 mm	Initial gap 4.2 mm	Initial gap 4.9 mm
W: Control blade withdrawn	-1.0	3.8	3.2	0	0
H: Control blade halfway inserted	-4.4	5.4	15.2	5.6	2.0
F: Control blade fully inserted	-8.3	11.8	56.4	46.8	41.2

5. CONCLUSIONS

A neutronics, thermal-hydraulics and structural analyses of SiC-SiC channel box has been performed for three different positions of the control blade (fully withdrawn, half-inserted and fully inserted). The analyses considered a fuel assembly located in the central region of a BWR core, operating under normal conditions. The following conclusions can be drawn from this work:

1. A sharp fast neutron flux gradient (up to 35-40%) is expected to develop across the width of the SiC-SiC channel box when the control blade is fully inserted. The temperature gradient across the channel width is expected to be small (2-3°C).
2. The channel box undergoes lateral bending for all positions of the control blade. However, the time dependence of the bending behavior differs for the different control blade positions. For cases W and F, the channel box continues to straighten after undergoing bending during initial stages of the operation; for case H, the channel box continues to bend with a decreasing bending rate with time, reaching a practically stationary bent position during the later stage of operation.
3. The maximum bending was found for the fully inserted blade position (case F). Although this case seems most detrimental from the perspective of interference between the control blade and channel box, the risk of severe interference exists only during the initial operation (~ 1 month). During subsequent reactor operation this configuration of the control blade will lead to minimal or no interference.
4. As presented in Table 6, the SiC-SiC channel box is expected to have interference for small initial gap widths (< ~4.3 mm), which can inhibit the movement of the control blade through the fuel assembly, thus raising concerns about reactor operation and safety. However, the interference can possibly be mitigated by designing a larger initial gap width and "avoiding" fully inserted control blade positions during the initial reactor operation; however, further analysis with time dependent control blade positioning is needed to assess the mitigation potential.
5. The channel box reaches a maximum stress of 155 MPa. This maximum stress is lower than the ultimate tensile strength (~250 MPa) of SiC-SiC composites, but greater than the proportional limit stress (~90 MPa) [31]. Thus, matrix microcracking is expected but a fully developed, through wall crack may not occur. From a practical perspective, the SiC-SiC channel box should be able to perform its intended functions of hydraulic and mechanical separation of the fuel assemblies, although some micromechanical damage will accrue during the reactor operation.

Future work will focus on fuel assemblies located in other regions of the core, such as near the core edge, and will incorporate realistic control blade movement histories. Additionally, the bowing of the channel boxes would displace moderator and produce the thermo-hydraulic feedback, which could be analyzed.

Acknowledgments

This research was sponsored by the Advanced Fuels Campaign – Nuclear Technology Research and Development program of U.S. Department of Energy, Office of Nuclear Energy.

6. REFERENCES

1. Katoh, Y., et al., *Stability of SiC and its composites at high neutron fluence.* Journal of Nuclear Materials, 2011. **417**(1-3): p. 400-405.
2. Katoh, Y., et al., *Radiation effects in SiC for nuclear structural applications.* Current Opinion in Solid State and Materials Science, 2012. **16**(3): p. 143-152.
3. Terrani, K., *Accident tolerant fuel cladding development: Promise, status, and challenges.* Journal of Nuclear Materials, 2018.
4. Katoh, Y., et al., *Continuous SiC fiber, CVI SiC matrix composites for nuclear applications: Properties and irradiation effects.* Journal of Nuclear Materials, 2014. **448**: p. 448-476.
5. Johnson, S.C., R.E. Henry, and C.Y. Paik. *Severe accident modeling of a PWR core with different cladding materials*. in *Proceedings of the 2012 International Congress on Advances in Nuclear Power Plants-ICAPP'12*. 2012.
6. Sebe, F., et al. *Development of Transient and Safety Analysis Method for ATF With SiC*. in *2016 24th International Conference on Nuclear Engineering*. 2016. American Society of Mechanical Engineers.
7. Heerden, E.v., et al., *Modeling of accident tolerant fuel for PWR and BWR using MAAP5.* 2017.
8. Ikegawa, T., et al., *Performance evaluation of accident tolerant fuel claddings during severe accidents of BWRs.* in Proceedings of Top Fuel, 2018.
9. Yueh, K. and K.A. Terrani, *Silicon carbide composite for light water reactor fuel assembly applications.* Journal of Nuclear Materials, 2014. **448**: p. 380-388.
10. Horie, H., et al. *Severe Accident Analysis for Reactor Core Applying SiC to Fuel Claddings and Channel Boxes*. in *2018 26th International Conference on Nuclear Engineering*. 2018. American Society of Mechanical Engineers.
11. Yueh, K., *SiC Composite for Fuel Structure Applications*. 2017, Electric Power Research Inst.(EPRI), Charlotte, NC (United States).
12. Koyanagi, T. and Y. Kato, *Systematic Technology Evaluation Program for SiC based BWR Channel Box*. 2019, Oak Ridge National Lab.(ORNL), Oak Ridge, TN (United States).
13. Pasamehmetoglu, K., et al., *State-of-the-Art Report on Light Water Reactor Accident-Tolerant Fuels*. 2018, Organisation for Economic Co-Operation and Development.
14. Singh, G., et al., *Deformation analysis of SiC-SiC channel box for BWR applications.* Journal of Nuclear Materials, 2019. **513**: p. 71-85.
15. Kochunas, B., et al. *Overview of development and design of MPACT: Michigan parallel characteristics transport code*. in *Proceedings of the 2013 International Conference on Mathematics and Computational Methods Applied to Nuclear Science and Engineering-M and C 2013*. 2013.
16. Salko, R.K., R.C. Schmidt, and M.N. Avramova, *Optimization and parallelization of the thermal–hydraulic subchannel code CTF for high-fidelity multi-physics applications.* Annals of Nuclear Energy, 2015. **84**: p. 122-130.
17. Leppänen, J., *Serpent–a continuous-energy Monte Carlo reactor physics burnup calculation code.* VTT Technical Research Centre of Finland, 2013. **4**.
18. Hitachi, G.E.-. [cited 2019 August 26]; Available from: https://nuclear.gepower.com/fuel-a-plant/products/ge14.
19. Williamson, R., et al., *Multidimensional multiphysics simulation of nuclear fuel behavior.* Journal of Nuclear Materials, 2012. **423**(1): p. 149-163.
20. Abaqus, *Version 2018 Documentation.* Dassault Systemes Simulia Corporation, 2018.
21. Snead, L.L., et al., *Handbook of SiC properties for fuel performance modeling.* Journal of Nuclear Materials, 2007. **371**(1-3): p. 329-377.

22. CARTER, C., R. DAVIS, and J. BENTLEY, *Kinetics and Mechanisms of High-Temperature Creep in Silicon Carbide: II, Chemically Vapor Deposited.* Journal of the American Ceramic Society, 1984. **67**(11): p. 732-740.
23. Singh, G., K. Terrani, and Y. Katoh, *Thermo-mechanical assessment of full SiC/SiC composite cladding for LWR applications with sensitivity analysis.* Journal of Nuclear Materials, 2018. **499**: p. 126-143.
24. Katoh, Y., et al., *Observation and possible mechanism of irradiation induced creep in ceramics.* Journal of Nuclear Materials, 2013. **434**(1): p. 141-151.
25. Singh, G., et al., *Elastic Moduli Reduction in SiC-SiC Tubular Specimen after High Heat Flux Neutron Irradiation Measured by Resonant Ultrasound Spectroscopy*. 2019: Journal of Nuclear Materials.
26. Singh, G., et al., *Parametric Evaluation of SiC/SiC Composite Cladding with UO2 Fuel for LWR Applications: Fuel Rod Interactions and Impact of Nonuniform Power Profile in Fuel Rod.* Journal of Nuclear Materials, 2018. **499**: p. 155-167.
27. Ferroni, P., *Steady state thermal hydraulic analysis of hydride fueled BWRs*. 2006, Massachusetts Institute of Technology.
28. Collins, B., et al., *Stability and accuracy of 3D neutron transport simulations using the 2D/1D method in MPACT.* Journal of Computational Physics, 2016. **326**: p. 612-628.
29. Fensin, M.L., *Optimum Boiling Water Reactor Fuel Design Strategies to Enhance Reactor Shutdown by the Standby Liquid Control System*. 2004, University of Florida.
30. Gauld, I.C., *SCALE-4 Analysis of LaSalle Unit 1 BWR Commercial Reactor Critical Configurations*. 2000, Oak Ridge National Lab., TN (US).
31. Singh, G., et al., *Interlaboratory round robin study on axial tensile properties of SiC-SiC CMC tubular test specimens.* International Journal of Applied Ceramic Technology, 2018. **15**: p. 1334-1349.
32. Cantonwine, P., et al. *Channel Control-Blade Interference Management at LaSalle 1 and 2 during 2007 and 2008*. in *Proceedings of the Water Reactor Fuel Performance Meeting - WRFPM / Top Fuel 2009*. 2009. France.
33. Cantonwine, P., et al. *Channel–Control Blade Interference in GE Boiling Water Reactor, D-Lattice Plants with Zircaloy-2 Channels*. in *Proceedings of LWR Fuel Performance/TopFuel/WRFPM 2010*. 2010. Orlando, Florida, USA.
34. Garzarolli, F., et al., *BWR Fuel Channel Distortion.* Advanced Nuclear Technology International, 2011.